Distortionless MVDR Beamformer for Conformal Array GNSS Receiver

Han Li[1], Di He[1(✉)], Xin Chen[1], Jiaqing Qu[2], and Lieen Guo[3(✉)]

[1] Shanghai Key Laboratory of Navigation and Location-Based Services, Shanghai Jiao Tong University, Shanghai, People's Republic of China
{hanzai_1101,dihe,xin.chen}@sjtu.edu.cn
[2] Shanghai Radio Equipment Research Institute, Shanghai, People's Republic of China
[3] School of Mechanical and Electrical Engineering, Nanchang University, Nanchang, People's Republic of China
guolieen@163.com

Abstract. The minimum variance distortionless response (MVDR) beamforming technique and space-time adaptive processing (STAP) have been playing important roles in interference suppression of globe navigation satellite system (GNSS) receiver. However, the demand for conformal arrays is increasing these days and its characteristics will vitiate the traditional MVDR method. And on the other side, traditional MVDR based on STAP will inevitably distort the Beidou signal, which is unacceptable in high precision GNSS applications. To address the above issues, first, a conformal array signal processing model is proposed; and based on that, a distortionless MVDR method is proposed in this study. The simulation results show that the proposed method can not only suppress the interference better than the traditional MVDR, but also guarantee the Beidou signal to be undistorted.

Keywords: Conformal antenna array · Interference suppression · Distortionless STAP

1 Introduction

GNSS is one of the most powerful infrastructures that provide positioning, navigation and timing (PNT) service for users all over the world [1,2]. Currently, there are four operating GNSS, the Global Positioning System (GPS) of the United States, the Global Navigation Satellite System (GLONASS) of Russia, the Galileo of the European Union and the Beidou Navigation Satellite System (BDS) of China. The BDS is a versatile GNSS completely designed and constructed independently by China. The BDS III was officially put into use and provide positioning service to the world in 2020, marking the BDS has formally become a GNSS.

Similar to other existing GNSS, BDS is also designed to withstand a certain level ($10log_{10}10230 \approx 40\,\mathrm{dB}$) of radio frequency interference [3], which is

H. Gao et al. (Eds.): ChinaCom 2021, LNICST 433, pp. 220–234, 2022.
https://doi.org/10.1007/978-3-030-99200-2_18

achieved by the direct-sequence spread spectrum (DSSS) technique [4] and is capable of coping with the most common noise. However, the application environment in real life is not always ideal. In addition to the receiver thermal noise, unintentional and deliberate interferences exist under many circumstances and undermine the reliability of PNT. Common unintentional interferences include some specialized communication systems like DME, TACAN, DVB-T, and so on. The deliberate jammer is used in electronic warfare (EW) or to defend one's own privacy, especially through the personal privacy devices (PPDs). Related researches show that a single jamming device can disable GNSS signal reception over a range of several kilometers [5]. To address these situations and enhance the robustness of the GNSS receiver, variety of GNSS interference mitigation countermeasures have been developed in the past decades, such as inertial aiding using IMU, vector tracking technique and filtering technique [3,5]. Among them, the filtering technique is most frequently used in the GNSS receiver, which can be grouped into time, frequency, time-frequency and spatial-time domains. It has been proved in practice that the spatial-time domain filtering is the most powerful interference mitigation method in aforementioned methods [6]. The spatial-time adaptive filtering (STAP) techniques utilize the antenna array combined with FIR filters to adaptively rearrange the received signals at the antenna in a weighted sum version to steer the antenna array response beam pointing to the desired direction and nulls pointing to the undesired interferences, which allow the BDS signals to pass unchanged and suppress the jamming effectively. Obviously, the effectiveness of receiving BDS signals and rejecting interferences is determined by the weights of each delayed tap. Therefore, the core of STAP algorithm is the principle of calculating the weights. Different approaches have been developed to realize the objective, including minimum mean square error (MMSE), MVDR and power inversion (PI), and they work well on suppressing the interference with high power [7–9]. However, the FIR filters introduced in STAP lead to non-linearity phase response which in turn cause the distortion of the desired signals [10,11]. Previous experiments suggest that without special attention on this issue, the positioning error brought by STAP can be tens of meters [11]. Therefore, in high-accuracy GNSS applications, this issue must be taken into consideration. Among some methods proposed to reduce the biases in code and carrier phase [6,10,12], the method proposed in [13] guarantees phase linearity and zero biases in code and carrier phase measurements.

A conformal array is a kind of antenna array that conforms to its bearer's surface which is designed for better aerodynamic and hydrodynamic performance or aesthetic consideration [14]. Therefore, it can be very useful in many applications such as radar or BDS receiver for high-speed aircraft. While most of the traditional interference suppression techniques can not be applied for conformal array directly since they generally assume that all the antennas are omnidirectional element and have identical response pattern. However, due to the non-planar curvature of the bearer surface, directional element model should be adopted and different antenna usually has different orientation, which in turn leads to different response to the same signal on different antenna [15,16]. Furthermore,

it means that the element response function can not be separated as a common factor of the array manifold which is a conventional practice used in planar array analysis. Accordingly, the mathematical model for the signal receiving procedure must be modified to take the above non-ideal conditions into consideration. Research about conformal array signal processing mainly focus on pattern synthesis and DOA estimation. Less attention is paid to the interference suppression technique in conformal array. So in this study, an array signal processing model integrating the element response is proposed.

The remainder of this article is organized as the following sections. In Sect. 2, a traditional procedure of suppressing interference with linear array is introduced. Next in Sect. 3, an extended signal processing model applicable to conformal array is given, and based on that a distortionless MVDR method for conformal array is proposed and analyzed. Then in Sect. 4, some simulation results are demonstrated to prove the effectiveness of the proposed method on conformal characteristic and distortionless performance. Finally, Sect. 5 concludes the paper.

2 Interference Suppression Using Antenna Array

In this section, a planar antenna array is considered to illustrate the traditional interference suppression method for GNSS using STAP and MVDR. Meanwhile, a general array signal processing model is established. Before that, the generation of the Beidou B3I signal and barrage jammer is introduced.

2.1 Signal Generation

Beidou B3I Signal. The Beidou B3I signal is composed of ranging code and navigation message modulated on the carrier using BPSK [4], which can be expressed as

$$S_{B3I}(t) = A_{B3I}C_{B3I}(t)D_{B3I}(t)\cos(2\pi ft + \varphi_{B3I}) \tag{1}$$

Among them, A_{B3I} represents the amplitude of the B3I signal. $D_{B3I}(t)$ is the data code of the B3I signal. In this study, it is assumed that only the D1 navigation message is used. $C_{B3I}(t)$ is the ranging code modulated on the data code by direct sequence spread spectrum (DSSS). The chip rate of C_{B3I} is $10.23Mcps$ and the code length is 10230. The C_{B3I} is generated by truncating a Gold code which is the result of truncating and XORing two linear sequences G1 and G2. The G1 and G2 sequences are respectively derived from two 13-bit linear shift registers, and its period is 8191 chips. The code sequence generated by G1 is truncated with the last one chip, making it into a CA sequence with a period of 8190 chips. The CA sequence with a period of 8191 chips is generated by G2. The C_{B3I} with a period of 10230 chips is generated by means of Modulo-2 addition of CA and CB sequences. f represents the carrier frequency of the B3I signal, which is 1268.52 MHz, φ_{B3I} represents the carrier initial phase of the B3I signal [4]. From the above, it is derived that the bandwidth of the B3I signal is 20.46 MHz. The Beidou B3I signal generation process is shown in Fig. 1.

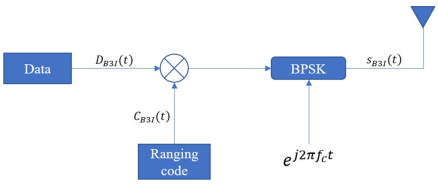

Fig. 1. Generation of the B3I signal.

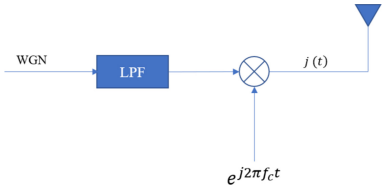

Fig. 2. Generation of the barrage jammer.

Interference. In this study, the interference is considered to be a barrage jammer covering the entire frequency band of B3I. To generate such a jammer. Firstly, a white Gaussian noise (WGN) is generated and passed through a low-pass filter with half of the bandwidth of the Beidou signal as passband bandwidth, and then the filter output signal is multiplied by the complex carrier signal $e^{j2\pi f_c t}$, modulated to the center frequency of B3I. The interference generation process is shown in Fig. 2.

2.2 Signal Receiving Model

Without loss of generality and for the sake of simplicity, an M-element omnidirectional linear array along with one B3I signal and K interference is considered. For a narrowband signal impinges from θ_k, its corresponding steering vector $\boldsymbol{a}$ is

$$\boldsymbol{a}(\theta_k) = [1 \quad e^{-j\phi_k} \ldots e^{-j(M-1)\phi_k}]^{\mathrm{T}} \tag{2}$$

where $[\cdot]^{\mathrm{T}}$ represents the transpose of a vector or matrix, ϕ_k is the phase delay due to propagation and can be expressed as

$$\phi_k = \frac{2\pi d_k}{\lambda} \sin\theta_k, \quad 1 \leq k \leq K \tag{3}$$

where d_k is the coordinate of the k-th antenna. Therefore, the observation vector $\boldsymbol{X}(n)$ of the array with dimension $M \times 1$ can be denoted as

$$\boldsymbol{X}(n) = \boldsymbol{a}(\theta_d)d(n) + \sum_{k=1}^{K} \boldsymbol{a}(\theta_k)j_k(n) + \boldsymbol{D}(n) \tag{4}$$

where $d(n)$ and $j_k(n)$ are the desired signal and the k-th interference, respectively [9]. Thus, $\boldsymbol{a}(\theta_d)$ and $\boldsymbol{a}(\theta_k)$ are the corresponding steering vectors. $D(n)$ is an $M \times 1$ vector representing the internal noise of the array.

Through a standard STAP implementation of P time taps, the final STAP observation vector can be expressed as

$$\boldsymbol{V}(n) = \begin{bmatrix} \boldsymbol{X}(n) \\ \boldsymbol{X}(n-1) \\ \vdots \\ \boldsymbol{X}(n-(P-1)) \end{bmatrix} \tag{5}$$

and the corresponding STAP steering vector $\boldsymbol{a_1} = \boldsymbol{a} \otimes \boldsymbol{a_t}$, ($\boldsymbol{a_t} = [1, e^{j2\pi f_c T_s}, \ldots, e^{j2\pi f_c (P-1) T_s}]^{\mathrm{T}}$, T_s is the sampling interval) [17], where $\otimes$ is the Kronecker product.

The filter coefficients of corresponding time taps also form an $MP \times 1$ vector $\boldsymbol{w} = [w_{11}, \cdots, w_{1P}, w_{21}, \cdots, w_{2P}, \cdots, w_{M1}, \cdots, w_{MP}]^{\mathrm{T}}$, where w_{mp} is the coefficient of the p-th delayed tap of mth element. Hence, the output y of the STAP filter is

$$y = \boldsymbol{w}^{\mathrm{H}} \boldsymbol{V} \tag{6}$$

2.3 Interference Suppression Using MVDR Beamformer

The MVDR beamformer minimizes the output signal power while maintaining the desired signal, which can be expressed in the following formulations [9]

$$\begin{cases} \min\limits_{\boldsymbol{w}} \boldsymbol{E}\{\|y\|^2\} = \min\limits_{\boldsymbol{w}} \boldsymbol{w}^{\mathrm{H}} \boldsymbol{R_{VV}} \boldsymbol{w} \\ \boldsymbol{w}^{\mathrm{H}} \boldsymbol{a_1}(\boldsymbol{\theta_d}) = 1 \end{cases} \tag{7}$$

$\boldsymbol{E}\{\cdot\}$ denotes the mathematical expectation, $\boldsymbol{R_{VV}}$ denotes the space-time covariance matrix defined as $\boldsymbol{R_{VV}} = \boldsymbol{E}\{\boldsymbol{V}\boldsymbol{V}^{\mathrm{H}}\}$. Using Lagrange multipliers, the object function can be expressed as

$$f(\boldsymbol{w}, \lambda) = \boldsymbol{w}^{\mathrm{H}} \boldsymbol{R_{VV}} \boldsymbol{w} + \lambda(\boldsymbol{w}^{\mathrm{H}} \boldsymbol{a_1} - 1) \tag{8}$$

and then the optimal coefficient vector $\boldsymbol{w}^{\star}$ can be acquired as

$$\boldsymbol{w}^{\star} = \frac{\boldsymbol{R_{VV}^{-1}} \boldsymbol{a_1}}{\boldsymbol{a_1}^{\mathrm{H}} \boldsymbol{R_{VV}^{-1}} \boldsymbol{a_1}} \tag{9}$$

3 Proposed Method

As mentioned above, the demand on the suppression based on the conformal antenna array is increasing. However, in traditional array signal processing, the radiation pattern function of all array elements are generally considered to be omnidirectional, and in this case, the global polar coordinate system is consistent with the local polar coordinate system of each array element. Therefore, the radiation function of the array element can be put forward as a common factor, which is called the Pattern Product Theorem (PPT), so that the radiation pattern of the array is only related to the geometric structure of the array. However, in the conformal array, firstly a directional antenna element model is more appropriate. Secondly, the different orientations of the array elements lead to the inconsistency between the global polar coordinate system and the local polar coordinate system of each array element, which makes the PPT fails and furthermore causes the error in signal array manifold estimation. So, the traditional beamforming algorithms do not work very well in the conformal antenna array structure.

In this section, a novel MVDR method based on Euler rotation is presented to solve the conformal array beamforming problem. Besides, the traditional STAP procedure is inevitable to introduce distortion on the desired signal due to the deployment of delayed time taps. Based on the conformal array beamforming above, a distortionless constraint is also introduced and analyzed in detail.

3.1 Conformal Array Signal Receiving Model

Here a more general conformal array model containing M elements is considered. In the global coordinate system, the position of each element is $\boldsymbol{p_i} = [x_i, y_i, z_i]^{\mathrm{T}}$, $(i = 1, 2, \cdots, M)$. For this array, first examine the synthesis of its array response pattern. Considering that a far-field narrow-band plane wave with a propagation direction of $\boldsymbol{a} = -[\sin\theta\cos\varphi \quad \sin\theta\sin\varphi \quad \cos\theta]^{\mathrm{T}}$ and wave length of λ_0 impinges on the array, so the corresponding wave vector is

$$\boldsymbol{k} = \frac{2\pi}{\lambda_0}\boldsymbol{a} \tag{10}$$

Among them, θ and φ are the elevation angle and azimuth angle in the global coordinate system. Furthermore, the radiation pattern of this array can be obtained

$$\boldsymbol{F}(\theta, \varphi) = \sum_{m=1}^{M} [w_m^* \boldsymbol{f_m}(\theta, \varphi) e^{-j\boldsymbol{k}^{\mathrm{T}}\boldsymbol{p_m}}] \tag{11}$$

where $\boldsymbol{f_i}(\theta, \varphi)$ is the radiation direction function of the i-th element itself, w_m is the corresponding complex weighting factor. Note that the global polar coordinate system is not consistent with local polar coordinate system of each element. To address this issue and for simplicity and generality, a five-element array with a central element conforms to a cylindrical surface is used for analysis. The specific array structure is shown in Fig. 3 below, all the elements point to the normal line. All elements have the same radiation function $\boldsymbol{f}(\theta, \varphi)$. Take p_i as an example to analyze its contribution to the array pattern. First, (θ, φ) is the polar coordinate corresponding to the global Cartesian coordinate system $O - xyz$, (θ_i, φ_i) is the coordinate in the polar coordinate system corresponding to the local Cartesian coordinate system $O_i - x_i y_i z_i$ of the ith array element. For a signal impinging from (θ, φ) in the global coordinate system, it first needs to be converted to local polar coordinate of each element, which can be achieved with Euler rotation.

It is known that the relationship between rectangular and polar coordinate system is

$$\begin{cases} x = \rho\sin\theta\cos\varphi \\ y = \rho\sin\theta\sin\varphi \\ z = \rho\cos\theta \end{cases} \tag{12}$$

where ρ is the distance between the signal source and the origin O. At the same time a new coordinate $O_i - x_i' y_i' z_i'$ is defined, which is generated by translate $O - xyz$ to make O overlap O_i

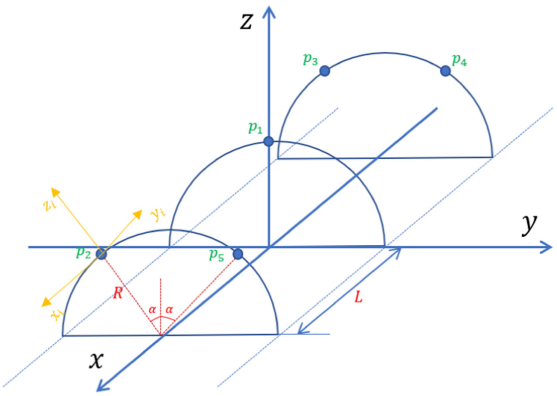

Fig. 3. Cylindrical conformal array structure.

$$\begin{bmatrix} x_i' \\ y_i' \\ z_i' \end{bmatrix} = \begin{bmatrix} x \\ y \\ z \end{bmatrix} - \boldsymbol{p_i} \tag{13}$$

It is obvious that $O_i - x_i y_i z_i$ can be generated by rotating $O_i - x_i' y_i' z_i'$ around O_i. Therefore, the relationship between the above two coordinates can be derived using Euler rotation [18] as follows

$$\begin{bmatrix} x_i \\ y_i \\ z_i \end{bmatrix} = R_x R_y R_z \begin{bmatrix} x_i' \\ y_i' \\ z_i' \end{bmatrix} \tag{14}$$

and for the cylindrical array proposed in Fig. 3, only the rotation of α° with $O_i x_i'$ as the rotation axis is needed. Then $\boldsymbol{R_y R_z} = \boldsymbol{I}$, combining with (13) and (14), the following transformation can be obtained

$$\begin{bmatrix} x_i \\ y_i \\ z_i \end{bmatrix} = \begin{bmatrix} 1 & 0 & 0 \\ 0 & \cos\alpha & -\sin\alpha \\ 0 & \sin\alpha & \cos\alpha \end{bmatrix} \begin{bmatrix} x - p_{ix} \\ y - p_{iy} \\ z - p_{iz} \end{bmatrix} = \begin{bmatrix} x - p_{ix} \\ (y - p_{iy})\cos\alpha - (z - p_{iz})\sin\alpha \\ (y - p_{iy})\sin\alpha + (z - p_{iz})\cos\alpha \end{bmatrix} \tag{15}$$

Besides, the signal is assumed to be far-field, so ρ can be regarded as $+\infty$. Using the definition of *arctan* function, local polar coordinate can be solved as

$$\begin{cases} \theta_i = \lim\limits_{\rho \to \infty} \arctan \dfrac{\sqrt{x_i^2 + y_i^2}}{z_i} \\ \quad = \arctan \dfrac{\sqrt{(\sin\theta\cos\varphi)^2 + (\sin\theta\sin\varphi\cos\alpha - \cos\theta\sin\alpha)^2}}{\sin\theta\sin\varphi\sin\alpha + \cos\theta\cos\alpha} \\ \varphi_i = \arctan 2(x_i, y_i) \end{cases} \tag{16}$$

where *arctan*2 function is the four-quadrant inverse tangent. Now the array radiation pattern can be transformed to

$$\boldsymbol{F}(\theta,\varphi)=\sum_{m=1}^{M}[w_m^*\boldsymbol{f}(\theta_m,\varphi_m)e^{-j\boldsymbol{k}^{\mathrm{T}}\boldsymbol{p_m}}] \tag{17}$$

As to the element radiation function, a cosine element model showed in Fig. 4 is used to better depict the radiation characteristic of elements on the convex conformal surface.

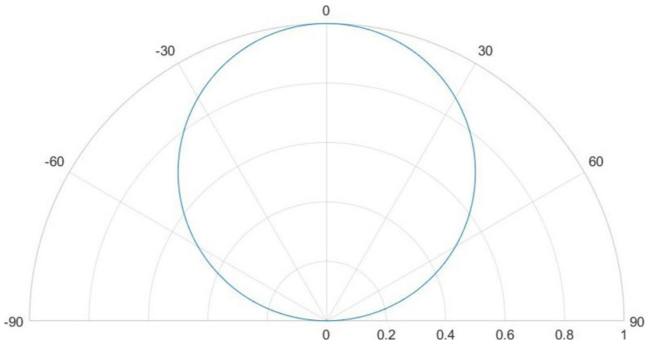

Fig. 4. Radiation pattern of the cosine element.

$$\boldsymbol{f}(\theta,\varphi)=\begin{cases}\cos\theta, 0\le\theta\le\frac{\pi}{2}\\ 0, \qquad else\end{cases} \tag{18}$$

Based on the above analysis, a general signal receiving model for an M-element convex conformal array can be obtained. Assume there are K interferences $j_k(t)(k=1,2,\cdots,K)$, and one B3I signal $d(t)$. For arbitrary signal $s(t)$ with incident angle of (θ,φ) and wave vector $\boldsymbol{k}$, its steering vector is

$$\boldsymbol{a}(\theta,\varphi)=[1,e^{-j\boldsymbol{k}^{\mathrm{T}}\overline{\boldsymbol{r_2}}},\cdots,e^{-j\boldsymbol{k}^{\mathrm{T}}\overline{\boldsymbol{r_M}}}]^{\mathrm{T}} \tag{19}$$

where $\overline{\boldsymbol{r_m}}=\boldsymbol{p_m}-\boldsymbol{p_1}$. Using the conversion in (16), the array response for $s(t)$ can be expressed as

$$\boldsymbol{x_s}=\begin{bmatrix}\boldsymbol{f}(\theta_1(\theta,\varphi))\\ \boldsymbol{f}(\theta_2(\theta,\varphi))\\ \vdots\\ \boldsymbol{f}(\theta_M(\theta,\varphi))\end{bmatrix}\boldsymbol{a}(\theta,\varphi)s(n)+\boldsymbol{D}(n) \tag{20}$$

Besides, the array manifold of the incoming signals can be expressed as

$$\boldsymbol{A}_{M\times(K+1)}=[\boldsymbol{a}(\theta_d,\varphi_d)\quad\boldsymbol{a}(\theta_{j_1},\varphi_{j_1})\quad\cdots\quad\boldsymbol{a}(\theta_{j_K},\varphi_{j_K})] \tag{21}$$

And for the convenience, the conformal factor matrix (CFM) $\boldsymbol{G}$ is defined to incorporate the conformal characteristic

$$\boldsymbol{G} = [\boldsymbol{g}(\theta_d, \varphi_d) \quad \boldsymbol{g}(\theta_{j_1}, \varphi_{j_1}) \cdots \boldsymbol{g}(\theta_{j_K}, \varphi_{j_K})] \tag{22}$$

where $\boldsymbol{g}(\theta, \varphi) = [\boldsymbol{f}(\theta_1(\theta, \varphi)), \cdots, \boldsymbol{f}(\theta_M(\theta, \varphi))]^{\mathrm{T}}$. Finally, the observation vector of the conformal array can be written as

$$\boldsymbol{X}(n) = \boldsymbol{G} \odot \boldsymbol{A} \begin{bmatrix} d(n) \\ j_1(n) \\ \vdots \\ j_K(n) \end{bmatrix} + \boldsymbol{D}(n) \tag{23}$$

where $\odot$ denotes the Hadamard product.

3.2 Distortionless MVDR Beamformer for Conformal Array

As mentioned above, a BDS signal is expected to pass the STAP filter without being distorted. To achieve this object, the output signal y_s of a single BDS signal with steering vector $\boldsymbol{a_d}$ after STAP filter is

$$\begin{aligned} y_s &= \sum_{m=1}^{M} \sum_{p=1}^{P} w_{m,p}^{*} c_{d,m} s\left(t - (p-1)T_s\right) \\ &= \sum_{p=1}^{P} \boldsymbol{w_p}^{\mathrm{H}} \boldsymbol{c_d} s\left(t - (p-1)T_s\right) \end{aligned} \tag{24}$$

where $\boldsymbol{c_d} = \boldsymbol{g}(\theta_d, \varphi_d) \odot \boldsymbol{a}(\theta_d, \varphi_d)$, and $\boldsymbol{w_p} = [w_{1,p}, w_{2,p}, \cdots, w_{M,p}]^{\mathrm{T}}$ denotes the weight vector at mth delayed tap, $[\cdot]^*$ denotes the conjugate operation. Actually, frequency response $H(f)$ of the STAP filter toward signal with steering vector $\boldsymbol{a_d}$ is in the same form [13]

$$H(f) = \sum_{p=1}^{P} \boldsymbol{w_p}^{\mathrm{H}} \boldsymbol{c_d} e^{-j2\pi f(p-1)T_s} = \sum_{p=1}^{P} h(p) e^{-j2\pi f(p-1)T_s} \tag{25}$$

It can be found that (25) is also equivalent to a FIR filter given in Fig. 5 with coefficient vector $h(p) = \boldsymbol{w_p}^{\mathrm{H}} \boldsymbol{c_d} \quad (p = 1, 2, \cdots, P)$.

Now, substitute the second constraint of the optimization problem (7) with (26) to guarantee the linearity of $H(f)$

$$\begin{cases} P \text{ is odd} \\ \boldsymbol{w}^{\mathrm{H}} \boldsymbol{c} = 1 \end{cases} \tag{26}$$

where $\boldsymbol{c} = \left[\underbrace{0 \cdots 0}_{M(P-1)/2} \quad \boldsymbol{c_d}^{\mathrm{T}} \quad \underbrace{0 \cdots 0}_{M(P-1)/2} \right]^{\mathrm{T}}$. Then the optimal weight can be solved using the Lagrange multipliers method introduced in Sect. 2.3 as

$$\boldsymbol{w}^{\star} = \frac{\boldsymbol{R_{VV}^{-1}} \boldsymbol{c}}{\boldsymbol{c}^{\mathrm{H}} \boldsymbol{R_{VV}^{-1}} \boldsymbol{c}} \tag{27}$$

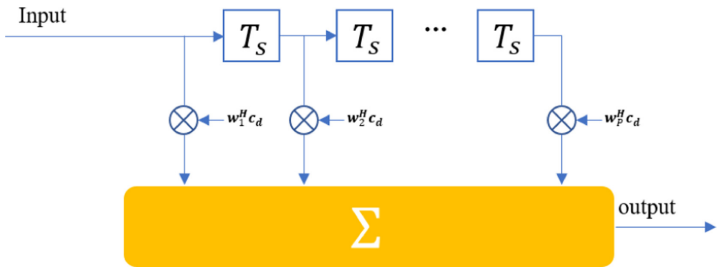

Fig. 5. Structure of the equivalent FIR filter.

The proof of this method applied on the traditional planar array has been detailed analyzed in [13]. Here the $\boldsymbol{a_s}$ in [13] is substituted by $\boldsymbol{c_d}$ which is the Hadamard product of $\boldsymbol{a_s}$ and $\boldsymbol{g}(\theta_d, \varphi_d)$. It is readily verified that this alteration does not affect the form and characteristic of $\boldsymbol{R_{VV}^{-1}}$ and $\boldsymbol{R_J}$ described in [13]. Finally, $\boldsymbol{h}$ can be obtained as

$$\boldsymbol{h} = \frac{\mu M}{\delta_n^2}\left[\frac{|\rho|^2\delta_n^2}{MP_J}r_{1,(P+1)/2} \quad \cdots \quad 1-|\rho|^2+\frac{|\rho|^2\delta_n^2}{MP_J}r_{(P+1)/2,(P+1)/2} \quad \cdots \quad \frac{|\rho|^2\delta_n^2}{MP_J}r_{P,(P+1)/2}\right]^{\mathrm{T}} \tag{28}$$

where δ_n^2, ρ, P_J denotes the noise variance, spatial correlation coefficient [19] between the desired signal and the interference, interference power, respectively. And more importantly, $\boldsymbol{h}$ is conjugate symmetric [13]. Combining that P is odd, the FIR filter coefficients meet the requirement of linear-phase system [20] with a constant bias $\frac{(P-1)T_s}{2}$. This bias does not affect the positioning accuracy because it remains the same for all incoming Beidou signals. Therefore, the proposed method is linear phased.

4 Simulation Results

In the simulation experiments, the array structure is the same as shown in Fig. 3 with $P = 5$, $R = 0.1\,\mathrm{m}$, $\alpha = 30°$, and $L = 0.1025\,\mathrm{m}$, and signals are generated based on the signal model given in Sect. 2, or by the procedure shown in Fig. 1 and Fig. 2. The received signals are down converted to intermediate frequency $f_{IF} = 46.52\,\mathrm{MHz}$ and then sampled with sampling rate $f_s = 62\,\mathrm{MHz}$, and sent to the TDLs where $T_s = 1/f_s$. The thermal noise power is $p_N = N_0 B$, where $B = 20.46\,\mathrm{MHz}$ is the bandwidth of Beidou B3I signal, $N_0 = k_B T_0$ is the noise power density, and k_B is the Boltzmann constant and T_0 is set to 290 K. The Beidou signal power used in the following simulations is set to SNR $= -30\,\mathrm{dB}$, and the jammer-noise ratio is set to JNR $= 70\,\mathrm{dB}$.

4.1 Interference Suppression Performance of the Proposed Method

The first experiment is used to demonstrate the interference suppression performance of the proposed method. One Beidou signal and one interference impinge from $(30°, 30°)$ and $(45°, 90°)$, respectively.

In Fig. 6, it shows the Power Spectral Density (PSD) of the signal received on $\boldsymbol{p_1}$ and that of the output signal. It is clear that the strong barrage jammer is dampened to the noise floor. From another perspective, if the signal received on any antenna is input into a standard Beidou receiver, the output would definitely be a garbled because the bit error rate (BER) is about 50%. While after the interference suppression, even though the desired signal mixed in the output signal is still overwhelmed by thermal noise, it can be decode by the standard Beidou receiver for the DSSS characteristic.

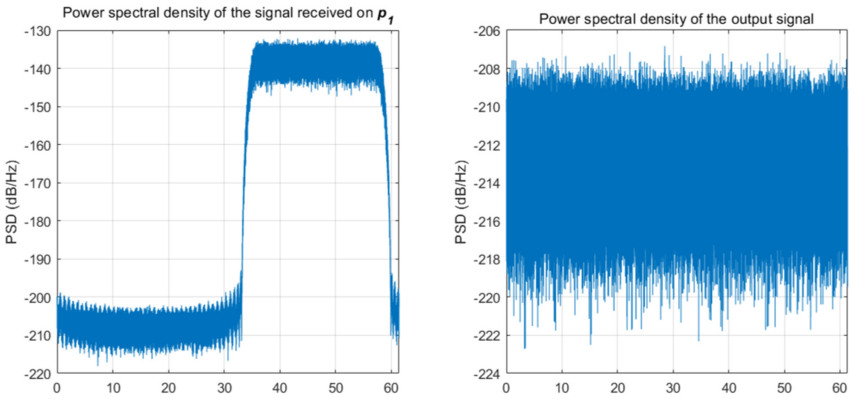

Fig. 6. PSD estimation comparision. The horizontal axis is the frequency in MHz.

From (17), the gain of the array at f is shown in Fig. 7. Obviously, a fairly deep null about $-121\,\mathrm{dB}$ is formed in the direction of the interference. While in the direction of the Beidou signal, there is about only $-0.04\,\mathrm{dB}$ attenuation. And the SINR is improved from about $-100\,\mathrm{dB}$ to about $-26\,\mathrm{dB}$, which can guarantee the receiver to decode correctly.

4.2 SINR Performance Comparison with the Traditional MVDR

Here a comparision experiment is adopted to prove that extra considerations on the antenna direction in the proposed method can help it outperform the traditional MVDR. In this simulation, the interference direction is fixed at $(45°, 90°)$, and the azimuth of the Beidou signal is fixed to 30°. Suppose the elevation angle varies from 0° to 90°, and the output signal SINR is plotted in Fig. 8.

As shown in Fig. 8, the output SINR of the traditional MVDR degrades faster than the proposed method as the altitude angle increases where the largest deficit

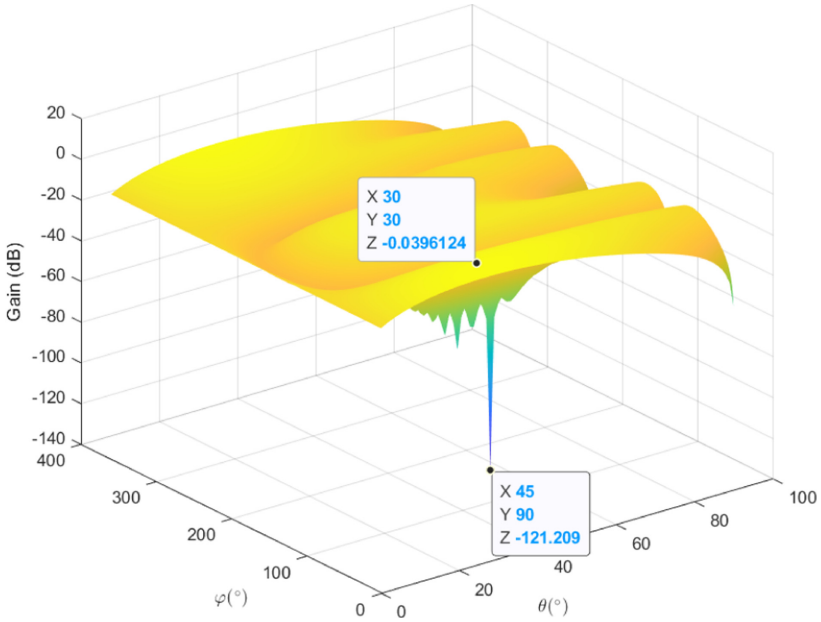

Fig. 7. Performance of array gain.

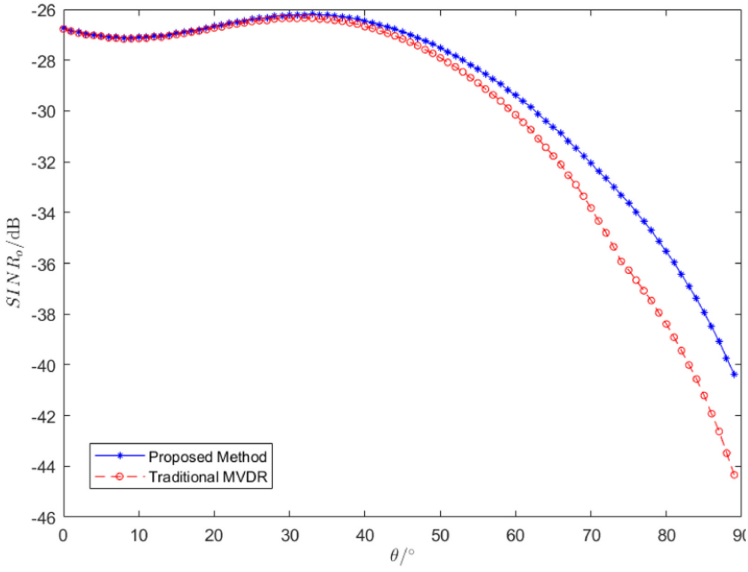

Fig. 8. SINR performance comparision.

can be up to 4dB when θ approaches 90°. This can be interpreted that mismatch of the signal steering vector gets larger as the elevation angle increases. Therefore, the proposed method has better estimation of the steering vector which enables a better SINR performance compared with traditional MVDR.

4.3 Beidou Signal Distortion Performance Comparison with the Traditional MVDR

Another comparision experiment is comparing the distortion between the proposed method and other commonly used methods including MVDR and PI. Here the cross-correlation function is used to measure the distortion. All the parameters are set as the same as in Sect. 4.1, but the weight coefficients are solved in different methods. And the result with the constant bias removed is shown in Fig. 9. Note that the ground truth curve is generated by sending the Beidou signal to the CCF directly.

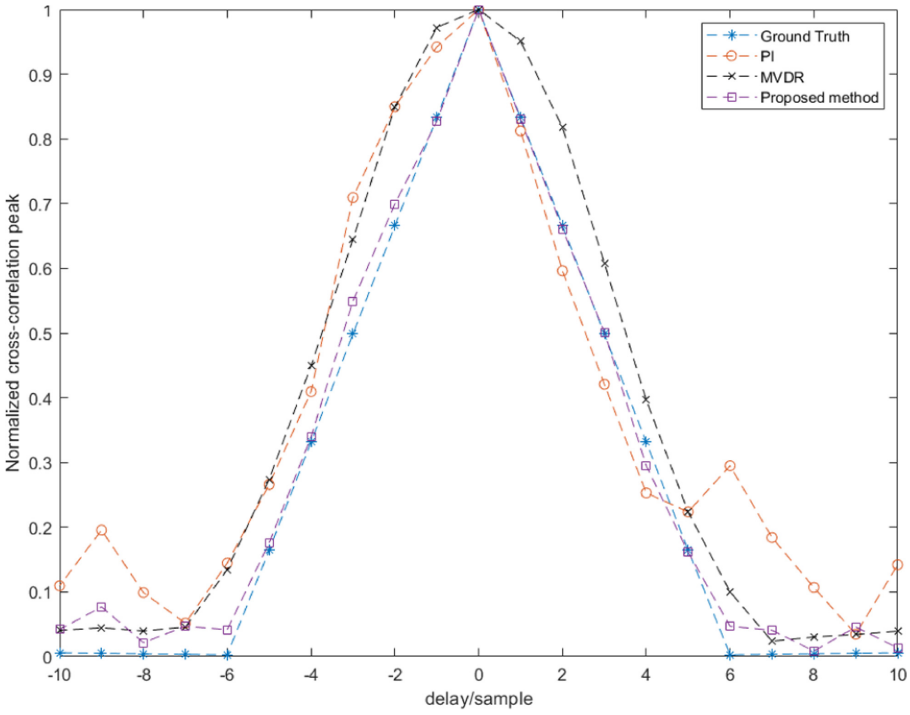

Fig. 9. CCF performance comparision.

As the figure illustrated, the most commonly used method, PI, would leads to a distortion in the cross-correlation peak significantly, undermine the symmetry in cross-correlation peak, and the MVDR method would broaden the

cross-correlation peak. The above phenomena in turn result in error in code phase estimation. On the contrary, the cross-correlation peak of the proposed method is quite close to the ground truth, indicating the desired signal is barely distorted.

5 Conclusion

A convex conformal array signal processing model is proposed in this study, and based on that a distortionless MVDR beamformer is introduced. The effectiveness of the proposed method is validated by theoretical analysis and numerical simulations. The results show that the proposed conformal array signal processing model can significantly improve the estimation of the steering vector and enhance the interference suppression performance. What's more, the results also show that the additional distortionless constraints can ensure the linearity of the STAP frequency response, maintain the Beidou signal and furthermore ensure the correct decoding of the standard receiver.

Acknowledgment. This research work was supported by the National Natural Science Foundation of China under Grant Nos. 61971278 and 61771308, the Joint Foundation of the Eighth Research Institute of China Aerospace Science and Technology corporation and Shanghai Jiao Tong University under Grant No. USCAST2020-26.

References

1. Xie, G., et al.: Principles of GPS and Receiver Design, vol. 7, pp. 61–63. Publishing House of Electronics Industry, Beijing (2009)
2. Borre, K., Akos, D.M., Bertelsen, N., Rinder, P., Jensen, S.H.: A Software-Defined GPS and Galileo Receiver: A Single-Frequency Approach. Springer, Boston (2007). https://doi.org/10.1007/978-0-8176-4540-3
3. Gao, G.X., Sgammini, M., Lu, M., Kubo, N.: Protecting GNSS receivers from jamming and interference. Proc. IEEE **104**(6), 1327–1338 (2016)
4. BeiDou navigation satellite system signal in space interface control document. http://www.beidou.gov.cn/xt/gfxz/201802/P020180209623601401189.pdf
5. Ioannides, R.T., Pany, T., Gibbons, G.: Known vulnerabilities of global navigation satellite systems, status, and potential mitigation techniques. Proc. IEEE **104**(6), 1174–1194 (2016)
6. Fante, R.L., Vaccaro, J.J.: Wideband cancellation of interference in a GPS receive array. IEEE Trans. Aerosp. Electron. Syst. **36**(2), 549–564 (2000)
7. Compton, R.: The power-inversion adaptive array: concept and performance. IEEE Trans. Aerosp. Electron. Syst. **6**, 803–814 (1979)
8. Van Veen, B., Buckley, K.M.: Beamforming techniques for spatial filtering. In: Digital Signal Processing Handbook, p. 61-1 (1997)
9. Van Trees, H.L.: Optimum Array Processing: Part IV of Detection, Estimation, and Modulation Theory. Wiley, Hoboken (2004)
10. Marathe, T., Daneshmand, S., Lachapelle, G.: Assessment of measurement distortions in GNSS antenna array space-time processing. Int. J. Antennas Propag. **2016**, 1–18 (2016)

11. O'Brien, A.J., Gupta, I.J.: Mitigation of adaptive antenna induced bias errors in GNSS receivers. IEEE Trans. Aerosp. Electron. Syst. **47**(1), 524–538 (2011)
12. Shuangxun, L., Zhu, C., Kan, H., Hongyin, X.: A compensating approach for signal distortion introduced by STAP. In: 2006 International Conference on Communication Technology, pp. 1–4. IEEE (2006)
13. Dai, X., Nie, J., Chen, F., Ou, G.: Distortionless space-time adaptive processor based on MVDR beamformer for GNSS receiver. IET Radar Sonar Navig. **11**(10), 1488–1494 (2017)
14. Hansen, R.: Conformal antenna array design handbook. Technical report, Naval Air Systems Command, Washington DC (1981)
15. Rasekh, M., Seydnejad, S.R.: Design of an adaptive wideband beamforming algorithm for conformal arrays. IEEE Commun. Lett. **18**(11), 1955–1958 (2014)
16. Zou, L., Laseby, J., He, Z.: Beamformer for cylindrical conformal array of non-isotropic antennas. Adv. Electr. Comput. Eng. **11**(1), 39–42 (2011)
17. Daneshmand, S.: GNSS interference mitigation using antenna array processing (2013)
18. Burger, H.A.: Use of Euler-rotation angles for generating antenna patterns. IEEE Antennas Propag. Mag. **37**(2), 56–63 (1995)
19. Lin, H.C.: Spatial correlations in adaptive arrays. IEEE Trans. Antennas Propag. **30**(2), 212–223 (1982)
20. Oppenheim, A.V.: Discrete-Time Signal Processing. Pearson Education India (1999)